VERSITA

Acta Geophysica
vol. 60, no. 5, Oct. 2012, pp. 1261-1286
DOI: 10.2478/s11600-011-0072-7

Vertical Structure of the Stable Boundary Layer Detected by RASS-SODAR and In-Situ Measurements in SABLES 2006 Field Campaign

Samuel VIANA[1], Carlos YAGÜE[2], and Gregorio MAQUEDA[3]

[1]Agencia Estatal de Meteorología (AEMET), Barcelona, Spain
e-mail: svianaj@aemet.es

[2]Departamento de Geofísica y Meteorología, Universidad Complutense de Madrid, Spain; e-mail: carlos@fis.ucm.es

[3]Departamento de Astrofísica y Ciencias de la Atmósfera, Universidad Complutense de Madrid, Spain; e-mail: gmaqueda@fis.ucm.es

A b s t r a c t

Data from the SABLES 2006 field campaign are used in order to analyse some of the main processes present along the nocturnal periods: surface-based inversions, low level jets, katabatic winds, wave-like motions, pressure perturbations, *etc*. These processes have an important influence on the vertical structure (both thermal and dynamical) of the atmospheric boundary layer, and can be better described with the synergetic combination of RASS-SODAR data and *in-situ* measurements (such as sonic anemometer data and high-resolution pressure series from microbarometers). It is shown how the different air masses and their evolution are easily identified when pressure and RASS-SODAR wind and temperature data are presented together. Likewise, periodic pressure fluctuations observed in the surface array of microbarometers reveal the existence of gravity wave motions whose propagation is better understood after locating the wave ducting layers with the help of RASS-SODAR average wind ant temperature profiles.

Key words: stable boundary layer, RASS-SODAR, gravity waves, pressure perturbations.

1. INTRODUCTION

The atmospheric boundary layer is usually defined as the fraction of the lower troposphere where an important transfer of physical properties (heat, momentum, mass, *etc*.) is produced between the atmosphere and the underlying surface in temporal scales of about one hour or less (Stull 1988, Arya 2001). One of its main characteristics is its turbulent character, which is generally continuous and very intense during the day. In contrast, after the sunset, the air becomes stable near the surface and turbulence can be sporadic and intermittent, leading to the appearance of complex phenomena that make difficult the study of the so-called Stable Boundary Layer (SBL). Several atmospheric phenomena are often present in the low atmosphere under these regimes, determining the evolution of the SBL along the night. Many of these features do not solely appear in the SBL, but their effects may be more important during this regime, as other forcings present in the daytime boundary layer disappear. Some relevant processes influencing the SBL, most of them not fully understood at present time, are related to: low-level jets (LLJ), elevated turbulence, wave generation and breaking, wave-turbulence interactions, slope flows, radiative flux divergence, intermittent turbulence (Klipp and Mahrt 2004, Mahrt 2010, Fernando and Weil 2010), *etc*. Important advances have been achieved recently, both in the experimental (Cuxart *et al.* 2000, Poulos *et al.* 2002, Grachev *et al.* 2005) and numerical simulations fields (Beare and McVean 2004, Beare *et al.* 2006, Cuxart *et al.* 2006). However, the physical processes controlling the development of the SBL as well as the turbulent mixing produced at different levels are far from being completely understood. Recently, Fernando and Weil (2010) have pointed out the need for understanding the nonlinear interactions of the different processes produced in the SBL, as well as the resulting modification in the transfer of heat, mass, and momentum.

Gravity waves stand out as one of these complex phenomena with a high level of variability and nonlinearity. In the atmospheric boundary layer, these are often produced when perturbations of different origin interact with stably-stratified atmospheric layers in the lower atmosphere (Nappo 2002), and they can be well monitored in the SBL, among other variables, through the study of pressure series. It has been previously reported that pressure fluctuations related to waves range in average between 0.01 and 0.1 hPa, with time scales between 1 and 40 min (Stull 1988). Nevertheless, some intense mesoscale events have been documented with higher amplitudes (*e.g*., Bosart and Cussen 1973, Viana *et al.* 2009). Although the linear theory can sometimes be applied to study the atmospheric waves present in the SBL (Gossard and Hooke 1975, Nappo 2002), most of these waves are far from a linear behaviour, and polarization relationships, as those between vertical

velocity and temperature ($\pi/2$ out of phase) which means that the vertical heat flux due to gravity waves is zero, are not always found. The interaction between turbulence and waves (Stewart 1969) is especially important for moderately to strongly stratified stable boundary layers, where no clear gap between turbulent and larger meso/submesoscale motions is present (Vickers and Mahrt 2003, Viana *et al.* 2007, 2009) and the turbulent fluxes evaluated from eddy-correlation technique with a fixed averaging window include a mixture of turbulence and wave-related processes.

Katabatic winds are non-stationary flows (Poulos *et al.* 2000, Martínez *et al.* 2010) produced when the surface cooling creates layers of denser air transported downslope. These winds can be present even for very small slopes (Barry 1992, Garratt 1992, Maguire *et al.* 2006) and are generally associated with weak pressure gradients. Their presence can change dramatically the stratification and the level of turbulence in the SBL.

Another frequent element in the SBL is the low-level jet (LLJ), characterized by a nocturnal wind maximum near the surface, which is often generated by inertial effects or sloping terrain (Stull 1988, Garratt 1992, Banta 2008). The presence of this phenomenon can be related to elevated turbulence (Banta *et al.* 2002, Conangla and Cuxart 2006) and generation of gravity waves (Viana *et al.* 2007, Cuxart 2008).

Some of the processes described above have been previously studied in the SBL by remote-sensing techniques, including SODAR measurements (Casadio *et al.* 1996, Murthy *et al.* 1996, Barlow *et al.* 2011). Kniffka *et al.* (2009) present statistical properties of SBL waves such as spatial coherences and frequency spectra determined by acoustic remote sensing methods, and estimate the anisotropy of the internal gravity waves. LLJs characteristics have been measured and analysed by SODAR in order to study their origin and behaviour (Kallistratova *et al.* 2009, Karipot *et al.* 2009) as well as to determine the SBL depth (Beyrich and Weill 1993, Beyrich 1994).

In the present paper, we concentrate on some of the above mentioned phenomena observed in the SABLES 2006 field campaign (Yagüe *et al.* 2007): slope flows, gravity waves, and LLJ. We will use data from the most common instrumentation in boundary-layer studies (sonic anemometers, low response instruments and microbarometers), showing the complementary information given by a RASS-SODAR. In Section 2, brief information on SABLES 2006 will be given. Three nights with different degree of turbulence and evolutions of the SBL will be analysed in Section 3. Finally some conclusions will be drawn.

2. FIELD CAMPAIGN

SABLES 2006 (Stable Atmospheric Boundary Layer Experiment in Spain) took place at the Research Centre for the Lower Atmosphere (CIBA in Span-

ish, 41°49′N, 4°56′W, 840 m asl) which is located around 30 km NW from Valladolid city in the center of the Duero basin, over a relatively flat, homogeneous high plain of nearly 800 km^2 elevated around 40-60 m above the plateau. As it has been shown from mesoscale models (Bravo *et al*. 2008, Cuxart 2008, Martínez *et al.* 2010), the nocturnal fair-weather flow at this high plain is the result of a complex set of drainage flows and mesoscale circulations of different scales which develop, interact and become organized within the Duero basin, as a result of the sheltering effect provided to this basin by the surrounding mountain ranges (see Fig. 1 in Cuxart *et al*. 2000). These circulations usually led to a northeast flow over the site (Cuxart *et al*. 2000, Yagüe *et al*. 2007).

Measurements took place in June and July 2006, including an intensive observation period (IOP) of ten consecutive nights from 21 June to 1 July. The purpose of SABLES 2006 was to study the SBL, with a focus on gravity waves and their interaction with turbulence. This objective was not possible in the former campaign, SABLES 98 (Cuxart *et al.* 2000), as microbarometers available at that moment failed during the campaign and the cup anemometers (in a triangular array) deployed to track and characterize waves had a too high starting threshold speed (offset), and most of the time were not able to provide useful information. A 100 m tower is available where standard instruments provide multiple levels of temperature (2.3, 10.5, 20.5, 35.5, and 97.5 m), wind speed and direction (2.3, 9.6, 34.6, 74.6, and 98.6 m), and humidity data (10, 97 m). Besides, 3 USA-1 sonic anemometers (measuring the three components of wind velocity as well as virtual temperature with a 20 Hz sampling rate) were deployed in the tower at 3, 19.6, and 96.6 m, as well as 6 Paroscientific microbarometers (3 installed at 20, 50, and 100 m on the tower, and 3 deployed at $z = 1.5$ m on a triangular array of 200 m side length approximately). These devices were configured to measure the absolute pressure at 2 Hz sample rate, which ensures a resolution around 0.002 hPa according to the manufacturer (both parameters are inversely related). Additional information on the operation of these devices can be consulted in Viana *et al.* (2007). The setup allows the detection and study of wave-like structures and the evaluation of wave parameters as period, wavelength, phase speed, and direction of propagation. Data from the RASS (Radio Acoustic Sounding System)/SODAR unit available at the site have been used to follow the evolution of the vertical structure of the SBL for a better characterization of some of the events studied in this work (*i.e*., LLJ, irruption of cold currents, shear regions, *etc*.), which improves in turn the information about the turbulent regime and wave-like structures extracted from the remaining instrumentation. SODARs produce acoustic pulses of a certain frequency which backscatter into the atmosphere; the frequency of the Doppler-shifted returning pulse is related to the radial velocity (the com-

ponents of the wind vector are obtained using three antennas aimed in orthogonal directions). On the other hand, RASS units can derive virtual temperatures by measuring sound velocities. These are extracted from the Doppler-shifted frequency of electromagnetic pulses which are backscattered on the acoustic fronts emitted from the SODAR as they propagate vertically (Pérez *et al.* 2008a).

The SODAR at CIBA is a DSDPA.90-24 METEK unit operating with 2.2 and 2.9 KHz sound frequencies, equipped with a RASS extension using 1290 MHz radio signals. Different papers have been published using data from this remote-sensing equipment in order to study the wind distribution at the site (Pérez *et al.* 2006, 2008a, b). The selected operating mode allows a vertical resolution of 20 m with a maximum vertical range of about 500 m. A plausibility code evaluates the data quality of the measurements according to the signal-to-noise ratio of the average power spectra; data were rejected according to standard criteria specified by the manufacturer. Data availability decreases with height and increases with averaging time: unless otherwise specified, 10-min averages have been used in this work, which means a typical availability of 90% below 220 m for the atmospheric nocturnal conditions present during the campaign. Further information on the RASS/SODAR model used in this campaign can be found in Engelbart *et al.* (1999). During the IOP, wind and temperature vertical profiles (reaching a maximum height of 300-900 m) were also obtained by a tethered balloon system with hourly soundings whenever winds were lower than 8 $m\,s^{-1}$ (for security reasons). Detailed characteristics of the instrumentation used in SABLES 2006 can be found in Viana *et al.* (2009, 2010).

3. RESULTS

3.1 Basic ABL parameters during the SABLES 2006 IOP

Figure 1a, b shows the evolution of temperature and the wind velocity modulus obtained from the tower measurements for the nights of the IOP. A time range from 18:00 to 06:00 GMT has been considered in order to include the transition from day to night and partially the morning transition (sunset was around 20:00 GMT and sunrise around 05:00 GMT during the IOP). A large surface cooling (more than 15 K) developed along most of the nights, which led to the formation of moderate to strong surface-based thermal inversions. One key point in the developing of the nocturnal processes is the intensity of the wind in the late afternoon. The evolution of the gradient Richardson number, Ri_g, and Turbulent Kinetic Energy, *TKE*, give an idea of the different degrees of stability and turbulence which are reached during this period (Fig. 1c, d). Gradient Richardson number is one of the most common stability parameters in the study of the SBL. Its importance lies in

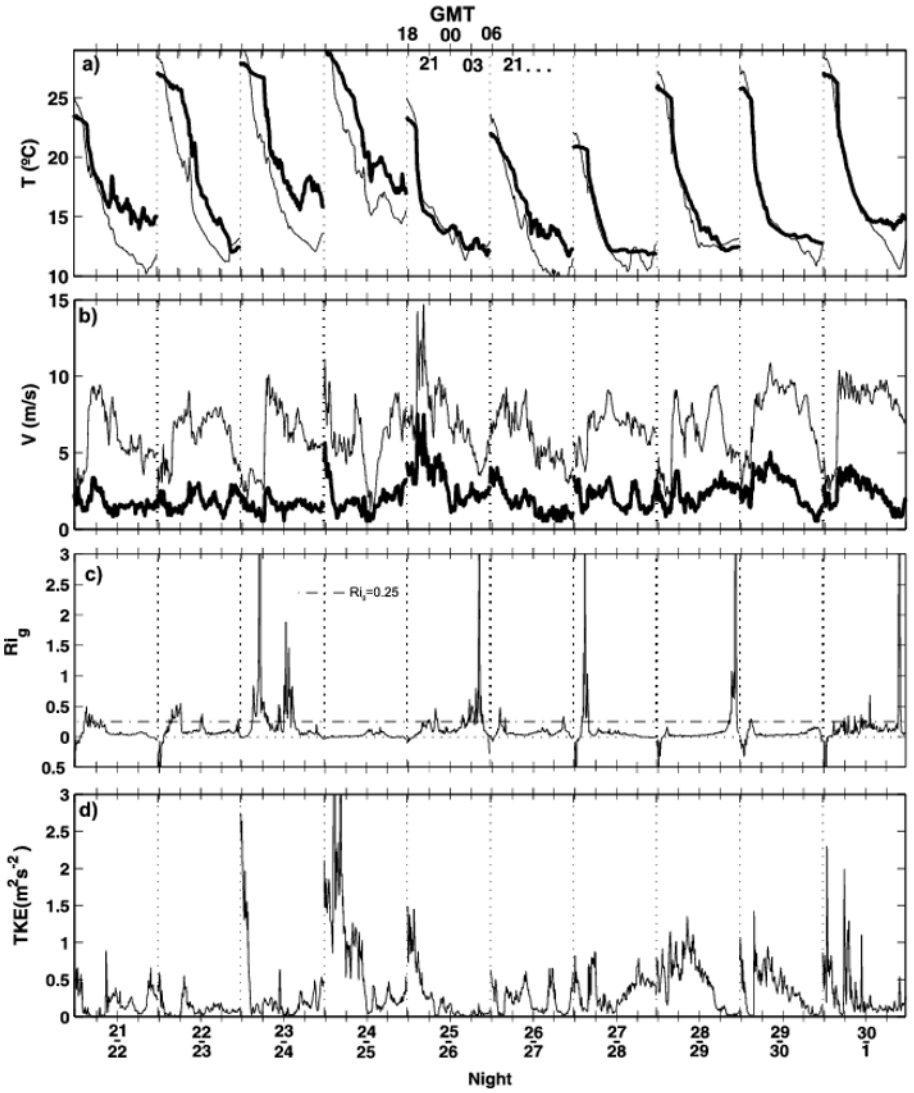

Fig. 1. Evolution along the 10 nights (18:00 to 06:00 GMT) of the IOP for: (a) temperature at 2.3 m (thin line) and 35.5 m (thick line), (b) wind speed at 98.6 m (thin line) and 2.3 m (thick line), (c) gradient Richardson number at $z = 3$ m, and (d) Turbulent Kinetic Energy at $z = 3$ m. Tick separation in the x-axis is three hours, and dotted vertical line indicates the change of night (*i.e.*, data from 06:00 to 18:00 GMT are not plotted).

that it takes into account both thermal stratification (in the SBL, acting in opposition to the development of turbulence) and wind shear (which generates turbulence):

$$Ri_g = \frac{\frac{g}{\theta_0}\frac{\partial \overline{\theta}}{\partial z}}{\left(\frac{\partial \overline{u}}{\partial z}\right)^2 + \overline{u}^2\left(\frac{\partial \overline{\alpha}}{\partial z}\right)^2}\ , \qquad (1)$$

which is equivalent to its traditional form considering both horizontal components of the wind (Stull 1988). In this expression, g is the acceleration due to gravity, θ the potential temperature, u the wind speed, and α the wind direction. These three meteorological variables have been obtained from log-linear fits to observations (in the case of potential temperature and wind speed) and linear fits (in the case of wind direction). Notice from the definition that the second term in the divisor is related to the gradient of the wind direction. This term is often ignored when evaluating the gradient Richardson number, as it is usually small inside the surface layer, but can be a significant contribution in SBLs where the surface layer is often only a few meters deep.

The evolution of the SBL at the CIBA site is quite similar some of the nights (nights of 21-22, 22-23, and those from 26-27 to 29-30), where the weak wind present at sunset allowed the developing of strong surface thermal inversions which were soon partially eroded by the turbulence generated by a katabatic wind reaching the site. These drainage flows, which have also been studied in the whole Duero basin from model simulations for similar synoptic conditions (Bravo *et al*. 2008, Martinez *et al.* 2010), are described in greater detail in Yagüe *et al*. (2007) and Viana *et al.* (2010). In the remaining nights of the IOP, drainage currents are weaker over the site and a moderate level of stratification prevails during the night (except the night of 24-25, where a well mixed boundary layer with nearly-neutral conditions is established due to a strong thunderstorm produced in the early evening).

3.2 Study of selected nights and processes

Katabatic flow

In this section we characterize the drainage current established during the night of 21-22 June from the combination of the RASS-SODAR and tower microbarometers. The evolution of wind direction, wind speed and temperature up to 200 m from 22:00 to 06:00 GMT is shown in Fig. 2a-c. These and the subsequent SODAR figures have been obtained directly from the graphic software provided by the manufacturer. A 10-min averaging window is used, and no post-processing is therefore applied, besides a slight smoothing to prevent excessive roughness in the contour lines.

Wind speed close to the surface increases around 22:30 GMT, and a few minutes later, the cold katabatic current irrupts in the site, when an abrupt

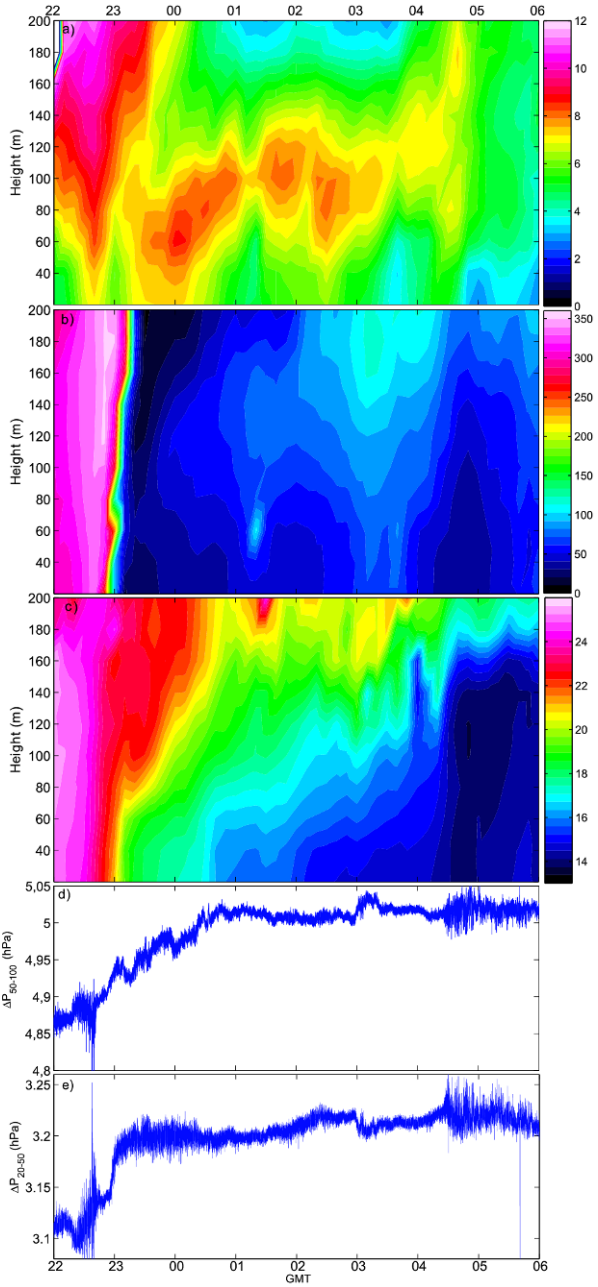

Fig. 2. Evolution of RASS-SODAR measurements for: (a) wind speed (in $m\,s^{-1}$), (b) wind direction (in degrees), (c) temperature (in °C), and (d)-(e) pressure differences between different tower microbarometers (50-100 and 20-50 m), from 22:00 to 06:00 GMT during the night of 21-22 June.

change in the wind direction from NW to NE is produced. The contouring process presents this change as a spurious veering (note that it lasts less than the 10-min averaging window). The RASS temperature (Fig. 2c) shows that the cooling starts close to the surface and propagates upwards, reaching levels above 200 m. The deepening of the cooled layer near the surface is probably a combination of drainage flows arriving at the CIBA and radiative cooling over an increasingly deep layer (as the temperature near the surface – 2.3 m – decreases monotonically along all the nights, except for some sporadic mixing events). These two processes could be identified from the wind speed and direction measurements: higher wind speeds at surface (drainage flows) or lower winds (radiative cooling). This is also inferred from pressure differences between tower levels (Fig. 2d, e), which reveal an abrupt increase of air density (*i.e*., cooling) between 20 and 50 m around 23:00 GMT, increasing more slowly between 50 and 100 m until approximately 00:30 GMT.

A well defined LLJ with its characteristic nose fluctuating at around 100 m is observed between 23:00 and 05:00 GMT (Fig. 2a). The picture resembles that of a classic cold front, as it was shown in Viana *et al*. (2010) for a similar night of the campaign. This "micro-front" can produce horizontal mass convergence inducing an upward motion which can be responsible for wave-like signals and even the generation of gravity waves in the separating layer between air masses. Unlike in the aforementioned case study, no clear evidences of gravity waves are present during this night, although some slow oscillations can be seen in Fig. 2d as the cold current thickens from 23:00 to 00:30 GMT.

The presented combination of SODAR and microbarometer data helps to better interpret the details in absolute pressure and pressure differences data. For instance, high frequency "noisy" pressure fluctuations like those appearing in Fig. 2e from 23:00 to 00:30 and from 04:30 to 06:00 GMT are typically related to turbulent activity somewhere in the air column between 20 and 50 m, but this can remain as pure speculation unless the turbulent layer coincides with the levels where the sonic anemometers are deployed. From Fig. 2a it is clear that the "noisy" fluctuations in $\Delta P_{20\text{-}50}$ match well with the periods where a strong wind shear is produced. The LLJ establishes around 23:00 GMT with its nose around 50 m, which increases the mean shear between 20 and 50 m as it is noticeable from the contour lines. After 00:30 GMT the wind maximum has risen above 80-90 m, therefore the wind shear between 20 and 50 m is smaller and the "noisy" fluctuations decrease. Likewise, from 04:30 to 06:00 GMT wind shear is strong again from 20 to 50 m due to nearly calm conditions close to the surface.

Strong stability, waves and turbulence

The night of 25-26 June was characterized by an increasing level of stratification along the night. Wind speed at sunset can be considered as moderate (Fig. 1b), and *TKE* is around 1.5 $m^2 s^{-2}$, one of the maximum values reached at 18:00 GMT for the 10 nights analysed (Fig. 1d). The evolution of the stability along the night in the layers close to the surface can be seen in Fig. 3, where the gradient Richardson number has been evaluated from tower data for the first 35 m from 18:00 to 06:00 GMT.

The initially unstable layer is stabilizing, from the lower to the higher levels, in the early hours of the night. Stability increases with height in the first few meters for most of the time, and high stability is achieved occasionally with supercritical Richardson numbers (> 0.25). The highest values are found from 02:00 GMT onwards, with extreme values at the lowest layers ($Ri_g > 2$) around 04:30 GMT. The RASS-SODAR images show a progressive cooling along the night with a clear surface-based inversion from midnight (Fig. 4c). A LLJ is detected lasting from 00:30 to 05:00 GMT, with maximum winds between 60 and 90 m agl (Fig. 4a), which compares well with the vertical wind speed soundings obtained at 02:00 and 03:00 GMT from the tethered balloon equipment (Fig. 5). Contrary to the previous night analysed (21-22), no katabatic irruption is appreciable on the microbarometers (not shown) or SODAR data. The wind direction data (Fig. 4b) shows a progressive clockwise veering of the wind from NW to NE and a maximum wind speed around 6 hours after sunset that could be related to the presence of an inertial oscillation linked to the establishment of the LLJ (again, the abrupt change

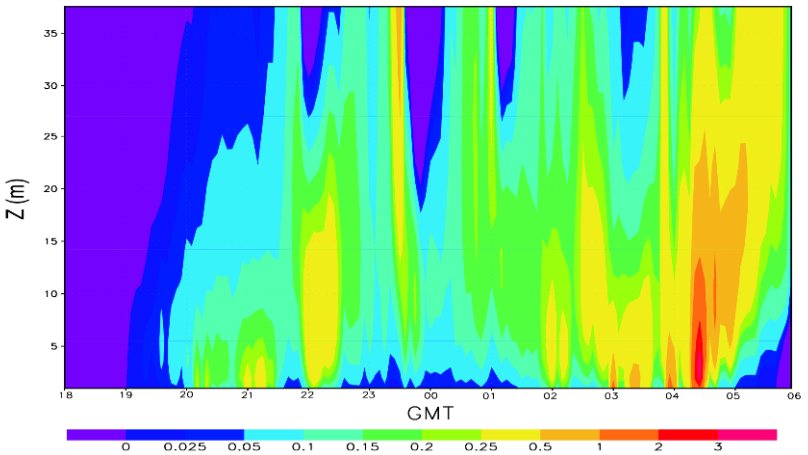

Fig. 3. Temporal evolution of the vertical structure of the gradient Richardson number along the 25-26 June night in the first 35 m. Colour version of this figure is available in electronic edition only.

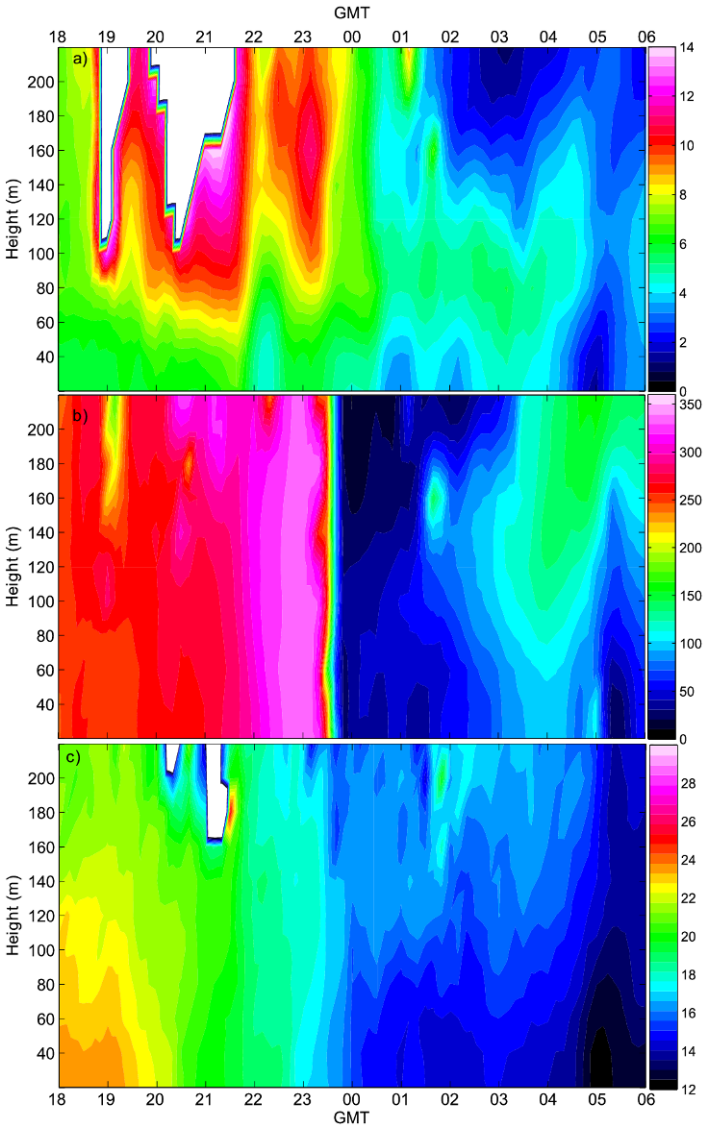

Fig. 4. Evolution of RASS-SODAR measurements for: (a) wind speed (in $m\,s^{-1}$), (b) wind direction (in degrees), and (c) temperature (in °C), from 18:00 to 06:00 GMT during the night of 25-26 June.

seen in SODAR right before 00:00 GMT is only an artefact of the contouring process). However, as Garratt (1992) mentions, in the real atmosphere is difficult to have the only presence of an inertial oscillation in the formation of a LLJ and other influences as changes in external conditions, sloping terrain,

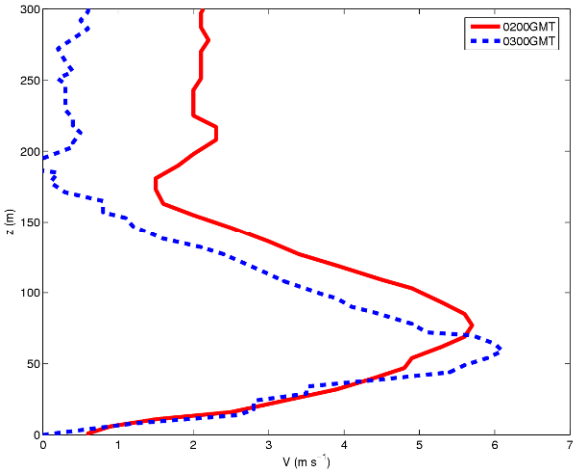

Fig. 5. Wind speed profiles obtained by tethered balloon on 26 June at 02:00 and 03:00 GMT. Colour version of this figure is available in electronic edition only.

advection and subsidence, mesoscale influences and gravity waves combine to produce more complicated behaviour. Cuxart (2008) studied in detail, from observations and mesoscale simulations, the possible origin of the LLJs at CIBA, and concluded that although sometimes an inertial oscillation can explain the initial formation, the topographic origin has a relevant role generating jets from the mountain ranges (100 km far from the CIBA) to the center of the basin.

The stability along the second part of the night together with the shear produced by the LLJ favour the development of gravity waves that can break producing elevated turbulence (Mahrt 1999). In the following paragraphs, different wave-like signals found along this night will be analysed with the help of the wavelet transform (WT). This is a spectral tool which acts as a local Fourier decomposition. It provides a simultaneous representation of the series in the time and frequency domains, showing which frequencies or periods are present and when they are present (Daubechies 1992). For further details of the WT applied to SBL and the detection and evaluation of wave parameters the reader is referred to papers by Terradellas *et al.* (2001) and Viana *et al.* (2009, 2010).

Figure 6 shows the surface pressure perturbations from 01:00 to 05:00 GMT together with the wavelet transform (WT) energy density. A high pass filter (a first order Butterworth filter with a cut-off frequency $f = 1/3600$ s^{-1}) has been applied to microbarometer data in order to remove the synoptic component (any contribution from timescales larger than one hour is removed). This filter has a flat spectral response up to the cut-off

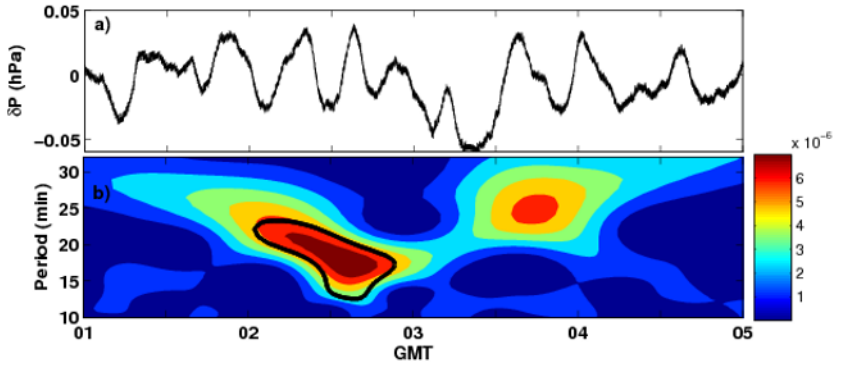

Fig. 6: (a) High-pass filtered surface pressure, and (b) WT energy density (in hPa^2s^{-1}) on 26 June (from 01:00 to 05:00 GMT). Colour version of this figure is available in electronic edition only.

frequency, which allows preserving all the characteristics from the pressure fluctuations. The profile of Ri_g below 35 m can help to understand what happens as the stability increases along the night (in the rest of the paper increase/decrease of stability should be interpreted as increase/decrease of Ri_g). From Fig. 3 it can be seen that, after 22:00 GMT, the strong level of stability ($Ri_g > 0.1$) that only affected to the first few meters above the surface, expands towards higher layers. After an interval in which the stability decreases slightly at all levels towards 23:30 GMT, there begins a period between 01:00 and 05:00 GMT in which the stability increases substantially, with frequent Richardson numbers above its critical value (0.25), especially close to the ground. A wave-like event propagating across the array of microbarometers at surface is detected between 02:00 and 03:00 GMT in the filtered surface pressure series, with a period between 17 and 20 min (area enclosed by a black contour line in Fig. 6b).

Another less significant maximum of a slightly longer period (20-25 min) appears between 03:30 and 04:00 GMT. Using a specific WT technique described in Viana *et al*. (2007), these features were shown to propagate towards SE with a phase speed $c = 7.5\text{-}9\ m\,s^{-1}$ and a wavelength $\lambda = 9\text{-}12$ km. Filtered pressure series from tower microbarometers prove to be very similar to those of the surface. This result, and the fact that pressure differences from different levels do not show any wave-like signal related to the one studied from surface, indicates that the wave originated and propagates well above 100 m but is felt by the microbarometers below that height due to the fact that pressure is not a local flow variable, but integrates the effects of the whole atmospheric layer above the measuring level. From the linear wave theory (Gossard and Hooke 1975) and with the help of SODAR data, it is possible to locate the layers where the wave is able to propagate. These

layers, known as "wave ducting layers" (Chimonas and Hines 1986), are bounded by critical levels which avoid a fast dissipation of the energy of waves which are eventually excited inside the ducting layer. The wave ducting layers are characterized by showing real values of the vertical wave number m:

$$m^2 = \frac{N_{BV}^2}{c_I^2} + \frac{\bar{U}_{zz}}{c_I} - k^2 - \frac{1}{4H_*^2} , \tag{2}$$

where $N^2 = (g/\theta)\,\partial\theta/\partial z$ is the square of the Brunt–Väisälä frequency, $c_I = c - U$ represents the intrinsic phase velocity (relative to the mean flow), U_{zz} is the second derivative with respect to height of the mean wind in the direction of propagation, and $H_* = RT/g$ is a height scale of the atmosphere (the last term in Eq. (2) is several orders of magnitude smaller than the rest and can be neglected). Figure 7 shows the vertical profile of the squared vertical wavenumber, evaluated using average RASS-SODAR wind and temperature profiles from 02:30 to 03:00 GMT and the wave parameters specified above. A surface-based wave ducting layer extends up to 130 m, but it is unlikely that the wave has been originated in the narrow layer extending from the top of the tower and the top of the wave ducting layer. We judge more likely the broader wave-ducting layer extending from 250 m and above as the region where the wave could originate and propagate horizontally. This wave-ducting layer could extend presumably well above 300 m, although the profile has not been evaluated above that height due to the lack of reliable wind data. Finally, it is worthwhile to note that SODAR average

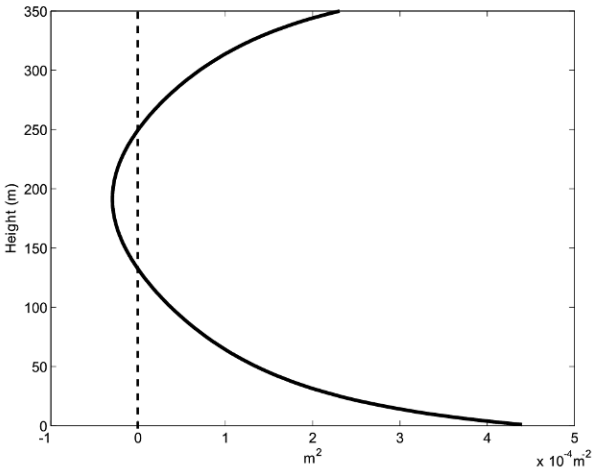

Fig. 7. Profile of the squared vertical wavenumber evaluated from RASS-SODAR data from 02:30 to 03:00 GMT.

profiles as those used for this application are much more suitable to study the wave-ducting process than the ones extracted from more instantaneous measurements such as the tethered balloon soundings, which tend to be sharper and more affected by transient perturbations, while waves are longer-lived, and their formation and propagation are thought to depend on the average background atmospheric conditions.

Vertical wind speed and temperature do not show significant wavelet energy over the temporal scales associated with the 20-min period structure. Nevertheless, other pulsating events of shorter duration and probably more local character are registered by the sonic anemometers at different levels of the tower. Temperature at 19.6 m shows a clear periodic fluctuation of up to 1 K magnitude from 02:15 to 02:30 GMT (Fig. 8a), just when Ri_g becomes supercritical at this level. The wavelet transform (Fig. 8b) reveals that its periodicity is well defined around 90 s, and coexists with a spectrum of faster

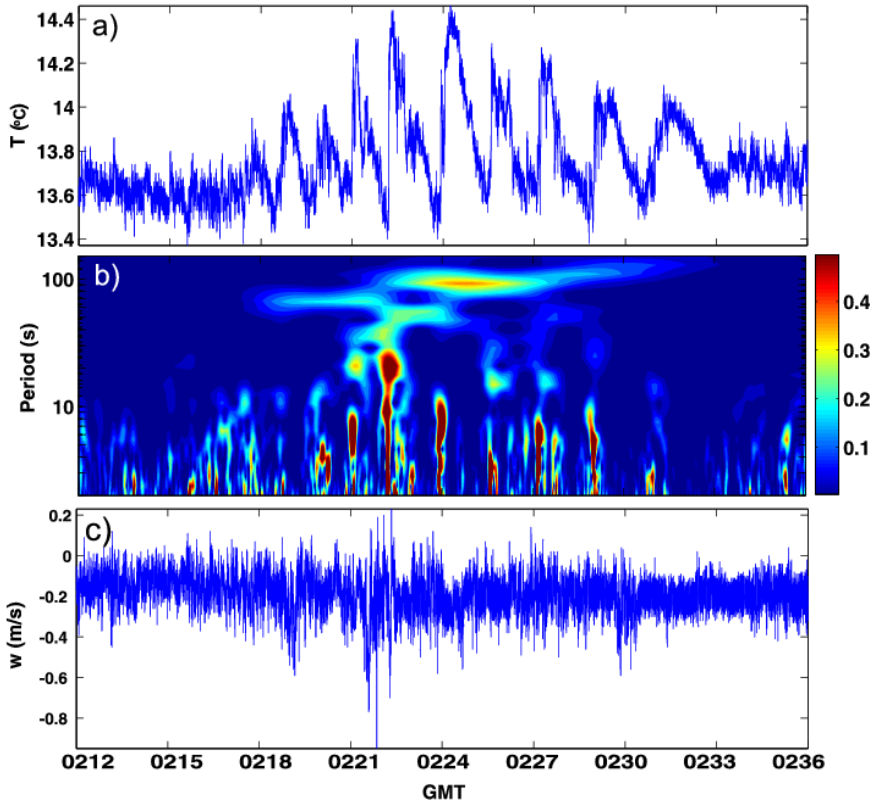

Fig. 8: (a) Sonic temperature at 19.6 m, (b) its wavelet energy density per period and time unit (in K^2s^{-1}), and (c) vertical velocity at 19.6 m for 26 June from 02:12 to 02:36 GMT. Colour version of this figure is available in electronic edition only.

turbulent contributions at timescales less than 10-20 s. This periodic event is not reflected at all in the vertical wind speed at $z = 19.6$ m (Fig. 8c) but, surprisingly, it is clearly mirrored at $z = 96.6$ m (Fig. 9a), with a similar periodicity but only in the vertical wind speed (Fig. 9b), showing a sharp temperature jump of nearly 1 K at this height (Fig. 9c), around 02:23 GMT when the event starts to weaken. This suggests a complex interaction between levels above and below the LLJ, which for the moment we have not been able to explain, but could be related to the non-linear interactions between different time scale structures ranging from 1 to 30 min. As Stull (1988) points out, weakly turbulent SBLs are filled with waves of different wavelengths and amplitudes which are superposed and sometimes break producing turbulence.

Another multiscale technique similar to the WT but highly appropriate for the turbulent scales, is the multiresolution decomposition (MR), where an

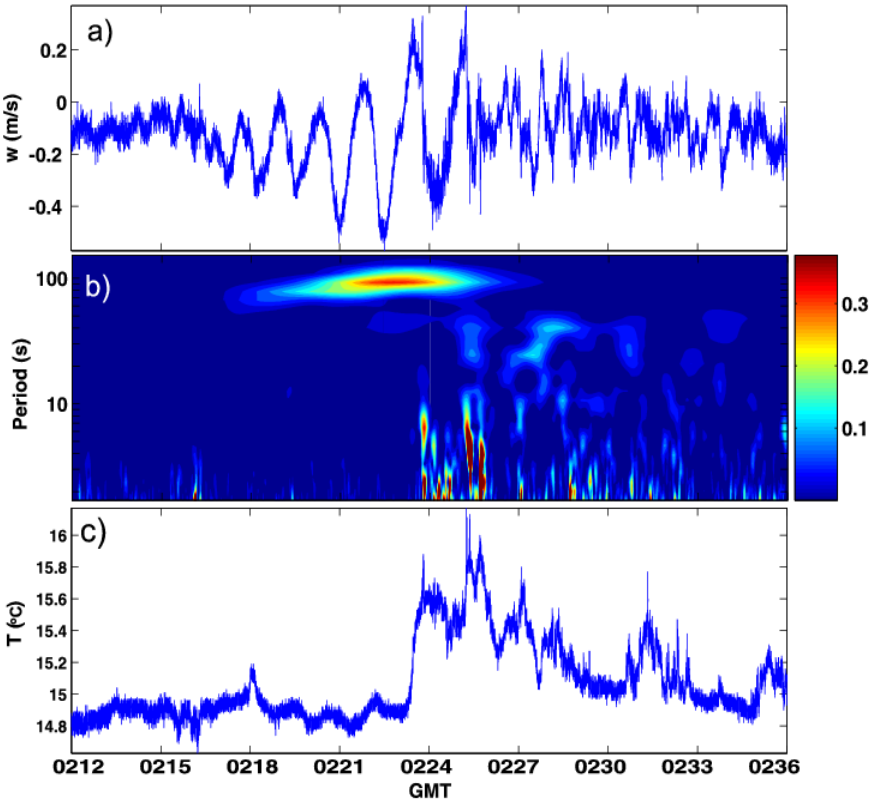

Fig. 9: (a) Vertical velocity at 96.6 m, (b) its wavelet energy density per period and time unit (in m^2s^{-3}), and (c) sonic temperature at 96.6 m for 26 June from 02:12 to 02:36 GMT. Colour version of this figure is available in electronic edition only.

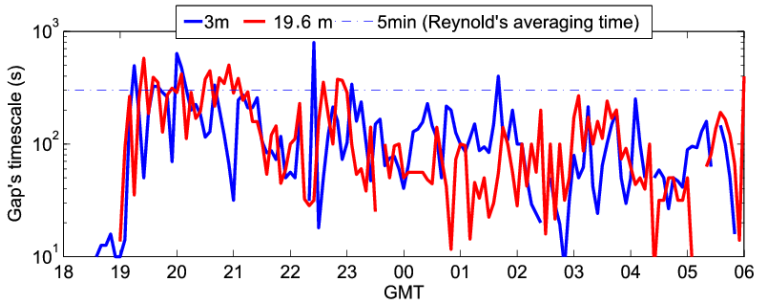

Fig. 10. Spectral gap evaluated at 3 and 19.6 m along the 25-26 night. The horizontal dashed line corresponds to 5 min. Colour version of this figure is available in electronic edition only.

orthogonal decomposition is used for computing turbulent fluxes (Howell and Mahrt 1997). If the MR is applied to vertical velocity and temperature series, then the turbulent heat flux can be obtained integrating the different MR coefficients from the minimum resolved time scale to the scale separating turbulent scales from larger ones (meso/submesoscales). This scale is usually referred to as "gap" or "spectral gap". The application of MR to turbulent fluxes is known as multiresolution flux decomposition (MRFD) and further details can be found in Vickers and Mahrt (2003) and Voronovich and Kiely (2007).

Figure 10 shows the temporal evolution of the gap throughout the night, at heights of 3 and 19.6 m. This gap has been evaluated by fitting every MR heat flux cospectra ($w\theta$) to a fifth-order polynomial, and locating the first occurrence of a zero crossing, an inflexion point or a minimum of the absolute value in the fitted cospectrum after the turbulent peak of maximum downward (negative) or upward (positive) heat flux (Voronovich and Kiely 2007). Due to the increase of stability, the vertical turbulent motions are inhibited, which reduces the average size of the turbulent eddies, their average timescale and the timescale of the gap separating turbulence from meso/submesoscales. At the beginning of the night (20:00 GMT), when the stability is weak and the SBL is still quite mixed, the gap at both heights is about 200-300 s. Later, in response to the increase of stability, the gap moves towards shorter timescales presenting differences between levels due to changes in the stability regime at both heights.

A general overview of the different contributions to the heat flux, obtained from MRFD at $z = 19.6$ m, for the most stable part of the night (from 00:00 to 06:00 GMT) is shown in Fig. 11. The strength of the downward (negative) heat flux in turbulent scales changes along the night and is closely linked to the level of stability: for example it decreases strongly from 04:00

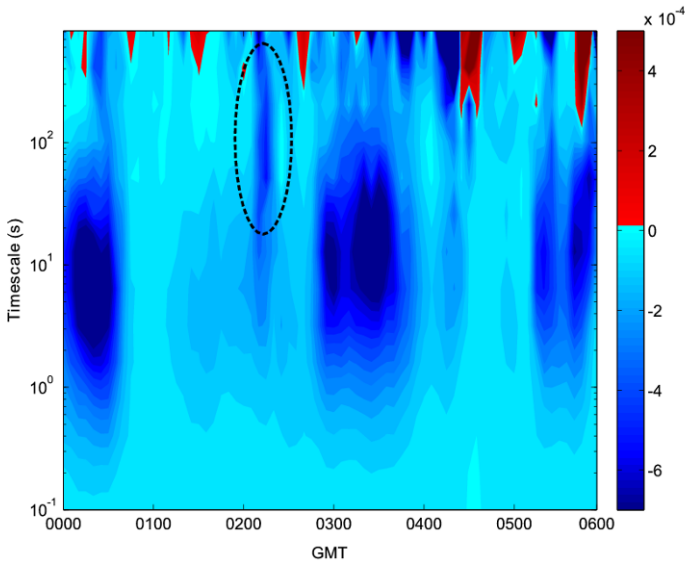

Fig. 11. The MR decomposition of the heat flux (in $\mathrm{K\,m\,s^{-1}}$) for different scales evaluated at z = 19.6 m from 00:00 to 06:00 GMT during the night of 25-26 June. Colour version of this figure is available in electronic edition only.

to 05:30 GMT, when a strong increase in Ri_g is present at 20 m (Fig. 3). On the other hand, the periodic signal detected in temperature around 02:15 GMT with a 90 s period (Fig. 8) produces a maximum contribution to the heat flux at these scales (see area enclosed by a dashed contour line). Counter-gradient fluxes, which are an indication of the presence of gravity waves (Nai-Ping *et al.* 1983, Viana *et al.* 2010) are found intermittently along the night for the larger scales (see red colours).

Finally, the contributions of three different ranges of periods (1-5, 5-10, and 10-30 min) to the heat flux have been evaluated from WT for 26 June (from 00:00 to 04:30 GMT). See Cuxart *et al.* (2002) for the methodology used. The results at z = 19.6 m are shown in Fig. 12. These fluxes are evaluated (from WT) each minute along the night. It can be seen that the heat fluxes for scales between 10-30 min have maximum values coinciding with the two events where the wavelet energy (Fig. 6) presented high values for the pressure series (around 02:15 GMT and for the interval 03:15-04:30 GMT). Although the bulk of the wave is believed to propagate over higher levels, gravity wave pressure perturbations can be transmitted to lower layers through the atmospheric column, producing effects close to the ground due to the altered horizontal pressure gradient, as in Viana *et al.* (2009). On the other hand, the flux contributions in the 5-10 min range are almost negligible most of the night. These are predominantly non-turbulent

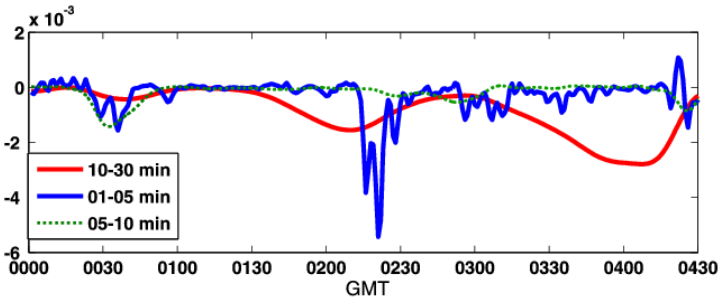

Fig. 12. Contribution to heat flux at 19.6 m (26 June, 00:00-04:30 GMT) from different period ranges. Colour version of this figure is available in electronic edition only.

flux contributions (the gap is around or below 5 min for most part of the night, as it was shown in Fig. 10), which implies that taking 5 min as an average for the calculations of turbulent fluxes for the eddy-covariance technique is not so bad *a priori*. We think that this lacking in energy between 5 and 10 min is quite interesting as a result as it supports the time window often used in the eddy-covariance (EC) technique to evaluate turbulent fluxes.

Analysing the smallest scales (periods of less than 5 min) reinforced the previous result (Fig. 11) that showed an increase in downward heat flux between 02:15 and 02:30 GMT, related to the 90 s period structure found on temperature at 19.6 m (Fig. 8). Here, a connection to wave-turbulence interaction may be established. This happens when, in the wavelet transform for pressure, an important contribution is seen at scales around 20 min; that is to say, the presence of major scales influences much lower scales and their corresponding fluxes (periods between 1 and 5 min). This interaction is related to the formation and breaking of waves, producing intermittent turbulence. The turbulence generated by the wave breaking is not of such a high frequency as the turbulence associated to weak stability situations where we have predominance of periods of less than 1 min, while in the accompanied cases of waves there are contributions of major periods (1-5 min). Regarding the second event (03:30-04:30 GMT), where higher stability is present (see Ri_g in Fig. 3) we believe that a clear wave-turbulence interaction is found, as the elevated turbulence is present (Ri_g is greater at 3 m than at 20 m).

Intermittent turbulence and stability

The 30 June – 01 July night presents a completely different evolution compared to other nights of the IOP. This night, the SBL is characterized by a high intermittency in the turbulence and stability. Sharp changes in tem-

perature, wind, Ri_g, and *TKE* take place from 18:00 to 00:00 GMT (Fig. 1). The RASS-SODAR (Fig. 13) shows a very weak wind from W at the late evening, suddenly veering N and NE and intensifying up to at least 220 m

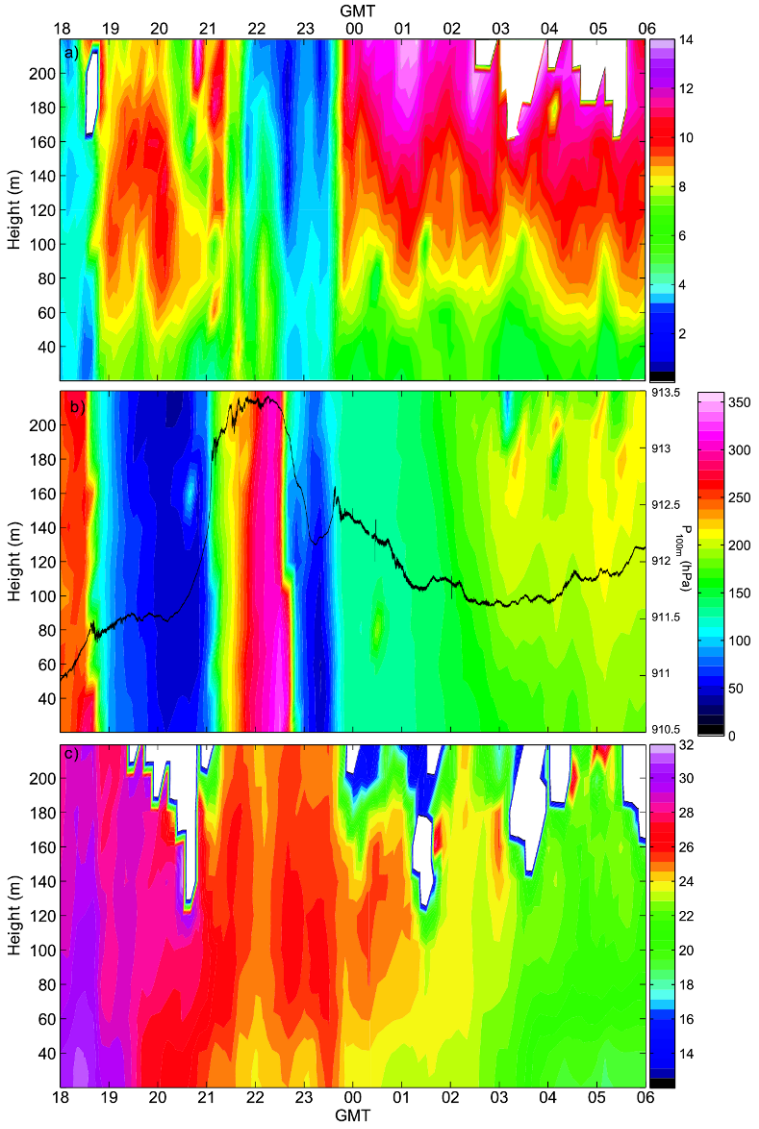

Fig. 13. Evolution of RASS-SODAR measurements for: (a) wind speed (in $m\,s^{-1}$), (b) wind direction (in degrees) and absolute pressure at $z = 100$ m (black line, right axis), and (c) temperature (in °C), from 18:00 to 06:00 GMT during the night of 30 June – 1 July.

around 18:30 GMT. A LLJ develops between 19:00 and 21:00 GMT, and temperature decreases 2 K on average during this period.

This veering and cooling could be related with the irruption of a katabatic wind as in the first night analysed here or that studied in Viana *et al.* (2010). However, in this case it appears very early in the night and it appears to homogeneously affect a very thick layer of at least 220 m. This might be related to a different configuration of the mesoscale circulations which are established in the basin, the weak winds prevailing at the site during the afternoon, or the combination of both factors. At 21:00 GMT, a slower change in wind direction from NE to SW takes place, and new veerings together with sharp changes in wind speed are produced afterwards until around 00:00 GMT. As it is apparent from Fig. 13b, these veerings coincide in time or are preceded by strong fluctuations up to 1.5-2 hPa in absolute pressure, suggesting that a variety of air masses from different origin are interacting in the area.

For the rest of the night (23:30 to 05:00 GMT) the wind direction remains without important changes, and a clear wind shear is produced between surface and higher levels. Surface cooling develops along this period, as well as wind oscillations, which are clearly visible from the RASS-SODAR (Fig. 13a) if we look at the 80 m level. These wind oscillations could be associated to the filtered pressure perturbations observed at those hours which are quite different from those produced from 18:00 to 23:30 GMT (not shown). The RASS-SODAR supply very useful information of the complex vertical structure of the nocturnal boundary layer and identify with high accuracy the sharp changes taking place along the night.

4. SUMMARY AND DISCUSSION

Data from SABLES 2006 field experiment have been used in this work to analyse the vertical structure of the nocturnal atmospheric boundary layer presenting very often stable stratification. An important support offered by the RASS-SODAR measurements has been shown in order to detect and study some of the typical phenomena developed along the SBL, as the presence of surface-based thermal inversions, low level jets, katabatic winds, gravity waves, intermittent turbulence, *etc*. Different nocturnal evolutions of the SBL where found for the 10 consecutive nights belonging to the IOP of the campaign. One of the most recurrent structures is the development of katabatic winds (21-22 June night) which is associated to a strong surface cooling developed after sunset and low winds at the transition time between the diurnal and nocturnal boundary layers. These katabatic winds produce a sharp increase in wind speed and veering of the wind direction, generally from NW to NE, decreasing significantly the temperature in the lower layers,

and inducing important bursts of turbulence. Another effect of the irruption of the katabatic winds on the SBL is the generation of wave-like perturbations. These were often registered by the microbarometers deployed at CIBA during the field campaign. The analysis of both the pressure perturbations and pressure differences between tower levels, and their combination with RASS-SODAR measurements has shown to be a very powerful tool to detect and characterize structures of different temporal scales developed along the night. A different nocturnal evolution of the SBL is obtained when the wind speed at sunset is not so weak (25-26 June night); in this case a progressive cooling of the surface is produced, with strong stability spreading along the SBL during the night. The presence of stably-stratified layers with the wind shear associated to the LLJ, make it possible to generate wave-like perturbations, which can present a very complex structure; these structures can be analysed with the help of the wavelet transform and mutiresolution techniques. The evolution of the spectral gap separating turbulent from larger meso/submesoscale motions gives useful information about the periods of the night in which non-turbulent scales fall below the temporal window usually used to evaluate turbulent fluxes from the EC method (300 s). For these cases, associated to high stability, the turbulent fluxes evaluated from EC are prone to be contaminated by submeso motions. Sometimes, large pressure perturbations are registered (30 June – 1 July night) associated to strong changes in wind direction; however, these large amplitude perturbations are not necessarily associated to the development of gravity waves, but to the changing advection of air masses from different directions and temperatures, as it is detected by the RASS-SODAR. It is not possible, however, from single point measurements at the CIBA site to obtain evidences of the circulations which generated, which should be studied from a larger mesoscale analysis using field observations and modelling, and we will try to work in this way in the future.

Acknowledgments. The authors wish to thank Dr. Javier Peláez, from the CIBA, for his technical support and help through the SABLES 2006 campaign. We are also grateful to Prof. J.L. Casanova, Director of the CIBA, for his support and help and to Prof. M.L. Sánchez from the Valladolid University for the RASS-SODAR data. This research has been funded by the Spanish Ministry of Science and Innovation (projects CGL2006-12474-C03-03 and CGL2009-12797-C03-03). The GR58/08 program (supported by BSCH and UCM) has also partially financed this work through the Research Group "Micrometeorology and Climate Variability" (No. 910437). The authors wish to thank the two anonymous referees for their useful comments.

References

Arya, S.P. (2001), *Introduction to Micrometeorology*, 2nd ed., Academic Press, London.

Banta, R,M. (2008), Stable-boundary-layer regimes from the perspective of the low-level jet, *Acta Geophys.* **56**, 1, 58-87, DOI: 10.2478/s11600-007-0049-8.

Banta, R.M., R.K. Newsom, J.K. Lundquist, Y.L. Pichugina, R.L. Coulter, and L. Mahrt (2002), Nocturnal low-level jet characteristics over Kansas during CASES-99, *Bound.-Layer Meteorol*. **105**, 2, 221-252, DOI: 10.1023/A: 1019992330866.

Barlow, J.F., T.M. Dunbar, E.G. Nemitz, C.R. Wood, M.W. Gallagher, F. Davies, E. O'Connor, and R.M. Harrison (2011), Boundary layer dynamics over London, UK, as observed using Doppler lidar during REPARTEE-II, *Atmos. Chem. Phys*. **11**, 2111-2125, DOI: 10.5194/acp-11-2111-2011.

Barry R.G. (1992), *Mountain Weather and Climate*, 2nd ed., Routledge, London.

Beare, R.J., and M.K. MacVean (2004), Resolution sensitivity and scaling of large-eddy simulations of the stable boundary layer, *Bound.-Layer Meteor.* **112**, 2, 257-281, DOI: 10.1023/B:BOUN.0000027910.57913.4d.

Beare, R.J., M.K. MacVean, A.A.M. Holtslag, J. Cuxart, I. Esau, J.C. Golaz, M.A. Jiménez, M. Khairoutdinov. B. Kosovic, D. Lewellen, T.S. Lund, J.K. Lundquist, A. McCabe, A.F. Moene, Y. Noh, A.S. Raasch, and P. Sullivan (2006), An intercomparison of large-eddy simulations of the stable boundary layer, *Bound.-Layer Meteorol.* **118**, 2, 247-272, DOI: 10.1007/ s10546-004-2820-6.

Beyrich, F. (1994), Sodar observations of the stable boundary layer height in relation to the nocturnal low-level jet, *Meteorol. Z.* **3**, 1, 29-34.

Beyrich, F., and A. Weill (1993), Some aspects of determining the stable boundary layer depth from sodar data, *Bound.-Layer Meteorol.* **63**, 1-2, 97-116, DOI: 10.1007/BF00705378.

Bosart, L.F., and J.P. Cussen, Jr. (1973), Gravity wave phenomena accompanying east coast cyclogenesis. *Month. Weather Rev.* **101**, 5, 446-454, DOI: 10.1175/1520-0493(1973)101<0446:GWPAEC>2.3.CO;2.

Bravo, M., T. Mira, M.R. Soler, and J. Cuxart (2008), Intercomparison and evaluation of MM5 and Meso-NH mesoscale models in the stable boundary layer, *Bound.-Layer Meteorol.* **128**, 1, 77-101, DOI: 10.1007/s10546-008-9269-y.

Casadio, S., A. Di Sarra, G. Fiocco, D. Fuà, F. Lena, and M.P. Rao (1996), Convective characteristics of the nocturnal urban boundary layer as observed with Doppler sodar and Raman lidar, *Bound.-Layer Meteorol.* **79**, 4, 375-391, DOI: 10.1007/BF00119405.

Chimonas, G., and C.O. Hines (1986), Doppler ducting of atmospheric gravity waves, *J. Geophys. Res*. **91**, 1219-1230, DOI: 10.1029/JD091iD01p 01219.

Conangla, L., and J. Cuxart (2006), On the turbulence in the upper part of the low-level jet: an experimental and numerical study, *Bound.-Layer Meteorol.* **118**, 2, 379-400, DOI: 10.1007/s10546-005-0608-y.

Cuxart, J. (2008), Nocturnal basin low-level jets: an integrated study, *Acta Geophys.* **56**, 1, 100-113, DOI: 10.2478/s11600-007-0042-2.

Cuxart, J., C. Yagüe, G. Morales, E. Terradellas, J. Orbe, J. Calvo, A. Fernández, M.R. Soler, C. Infante, P. Buenestado, A. Espinalt, H.E. Joergensen, J.M. Rees, J. Vilà, J.M. Redondo, I.R. Cantalapiedra, and L. Conangla (2000), Stable Atmospheric Boundary-Layer Experiment in Spain (SABLES 98): A report, *Bound.-Layer Meteorol.* **96**, 3, 337-370, DOI: 10.1023/A:1002609509707.

Cuxart, J., G. Morales, E. Terradellas, and C. Yagüe (2002), Study of coherent structures and estimation of the pressure transport terms for the nocturnal stable boundary layer, *Bound.-Layer Meteorol.* **105**, 2, 305-328, DOI: 10.1023/A:1019974021434.

Cuxart, J., A.A.M. Holtslag, R.J. Beare, E. Bazile, A. Beljaars, A. Cheng, L. Conangla, M. Ek, F. Freedman, R. Hamdi, A. Kerstein, H. Kitagawa, G. Lenderink, D. Lewellen, J. Mailhot, T. Mauritsen, V. Perov, G. Schayes, G.-J. Steeneveld, G. Svensson, P.Taylor, W. Weng, S. Wunsch, and K.-M. Xu (2006), Single-column model intercomparison for a stably stratified atmospheric boundary layer, *Bound.-Layer Meteorol.* **118**, 2, 273-303, DOI: 10.1007/s10546-005-3780-1.

Daubechies, I. (1992), *Ten Lectures on Wavelets*, CBMS Lecture Notes Series. SIAM.

Engelbart, D., H. Steinhagen, U. Görsdorf, J. Neisser, H.J. Kirtzel, and G. Peters (1999), First results of measurements with a newly-designed phased-array sodar with RASS, *Meteorol. Atmos. Phys.* **71**, 1-2, 61-68, DOI: 10.1007/s007030050044.

Fernando, H.J.S., and J.C. Weil (2010), Whither the stable boundary layer?, *Bull. Amer. Meteor. Soc.* **91**, 1475-1484, DOI: 10.1175/2010BAMS2770.1.

Garratt, J.R. (1992), *The Atmospheric Boundary Layer*, Cambridge University Press, Cambridge.

Gossard, E., and W.H. Hooke (1975), *Waves in the Atmosphere*, Elsevier, New York, 456 pp.

Grachev, A.A., C.W. Fairall, P.O.G. Persson, E.L. Andreas, and P.S. Guest (2005), Stable boundary-layer scaling regimes: The SHEBA data, *Bound.-Layer Meteorol.* **116**, 2, 201-235, DOI: 10.1007/s10546-004-2729-0.

Howell, J.F., and L. Mahrt (1997), Multiresolution flux decomposition, *Bound.-Layer Meteorol.* **83**, 1, 117-137, DOI: 10.1023/A:1000210427798.

Kallistratova, M., R.D. Kouznetsov, D.D. Kuznetsov, I.N. Kuznetsova, M. Nakhaev, and G. Chirokova (2009), Summertime low-level jet characteristics measured by sodars over rural and urban areas, *Meteorol. Z.* **18**, 3, 289-295, DOI: 10.1127/0941-2948/2009/0380.

Karipot, A., M.Y. Leclerc, and G. Zhang (2009), Characteristics of nocturnal low-level jets observed in the north Florida area, *Month. Weather Rev.* **137**, 8, 2605-2621, DOI: 10.1175/2009MWR2705.1.

Klipp, C.L., and L. Mahrt (2004), Flux-gradient relationship, self-correlation and intermittency in the stable boundary layer, *Quart. J. Roy. Meteor. Soc.* **130**, 601, 2087-2103, DOI: 10.1256/qj.03.161.

Kniffka, A., A. Ziemann, I. Chunchuzov, S. Kulichkov, and V. Perepelkin (2009), Anisotropy in internal gravity waves in conditions of a stable nocturnal boundary layer, *Meteorol. Z.* **18**, 3, 331-337, DOI: 10.1127/0941-2948/2009/0378.

Maguire, A.J., J.M. Rees, and S.H. Derbyshire (2006), Stable atmospheric boundary layer over a uniform slope: some theoretical concepts, *Bound.-Layer Meteorol.* **120**, 2, 219-227, DOI: 10.1007/s10546-006-9055-7.

Mahrt, L. (1999), Stratified atmospheric boundary layers, *Bound.-Layer Meteorol.* **90**, 3, 375-396, DOI: 10.1023/A:1001765727956.

Mahrt, L. (2010), Variability and maintenance of turbulence in the very stable boundary layer, *Bound.-Layer Meteorol.* **135**, 1, 1-18, DOI: 10.1007/s10546-009-9463-6.

Martínez, D., M.A. Jiménez, J. Cuxart, and L. Mahrt (2010), Heterogeneous nocturnal cooling in a large basin under very stable conditions, *Bound.-Layer Meteorol.* **137**, 1, 97-113, DOI: 10.1007/s10546-010-9522-z.

Murthy, B.S., T. Dharmaraj, and K.G. Vernekar (1996), Sodar observations of the nocturnal boundary layer at Kharagpur, India, *Bound.-Layer Meteorol.* **81**, 2, 201-209, DOI: 10.1007/BF00119065.

Nai-Ping, L., W.D. Neff, and J.C. Kaimal (1983), Wave and turbulence structure in a disturbed nocturnal inversion, *Bound.-Layer Meteorol.* **26**, 2, 141-155, DOI: 10.1007/BF00121539.

Nappo, C.J. (2002): *An Introduction to Atmospheric Gravity Waves*, Academic Press, London.

Pérez, I.A., M.A. García, M.L. Sánchez, and B. de Torre (2006), Fit of wind speed and temperature profiles in the low atmosphere from RASS sodar data, *J. Atmos. Sol-Terr. Phys.* **68**, 10, 1125-1135, DOI: 10.1016/j.jastp.2006.02.013.

Pérez, I.A., M.Á. García, M.L. Sánchez, and B. de Torre (2008a), Description of atmospheric variables measured with a RASS sodar: Cycles and distribution functions, *J. Wind Eng. Ind. Aerodyn.* **96**, 4, 436-453, DOI: 10.1016/j.jweia.2008.01.001.

Pérez, I.A., M.L. Sánchez, M.Á. García, and B. de Torre (2008b), Description and distribution fitting of transformed sodar wind observations, *J. Atmos. Sol.-Terr. Phys.* **70**, 1, 89-100, DOI: 10.1016/j.jastp.2007.10.004.

Poulos, G.S., J.E. Bossert, T.B. McKee, and R.A. Pielke (2000), The interaction of katabatic flow and mountain waves. Part I: Observations and idealized

simulations, *J. Atmos. Sci.* **57**, 12, 1919-1936, DOI: 1520-0469(2000)057 <1919:TIOKFA>2.0.CO;2.

Poulos, G.S., W. Blumen, D.C. Fritts, J.K. Lundquist, J. Sun, S.P. Burns, C. Nappo, R. Banta, R. Newsom, J. Cuxart, E. Terradellas, B. Balsley, and M. Jensen (2002), CASES-99: A comprehensive investigation of the stable nocturnal boundary layer, *Bull. Amer. Meteorol. Soc.* **83**, 4, 555-581, 10.1175/1520-0477(2002)083<0555:CACIOT>2.3.CO;2.

Stewart, R.W. (1969), Turbulence and waves in a stratified atmosphere, *Rad. Sci.* **4**, 12, 1269-1278, DOI: 10.1029/RS004i012p01269.

Stull, R.B. (1988), *An Introduction to Boundary Layer Meteorology*, Kluwer Academic Publishers, Dordrecht.

Terradellas, E., G. Morales, J. Cuxart, and C. Yagüe (2001), Wavelet methods: application to the study of the stable atmospheric boundary layer under non-stationary conditions, *Dyn. Atmos. Oceans* **34**, 2-4, 225-244, DOI: 10.1016/S0377-0265(01)00069-0.

Viana, S., C. Yagüe, G. Maqueda, and G. Morales (2007), Study of the surface pressure fluctuations generated by waves and turbulence in the nocturnal boundary layer during SABLES2006 field campaign, *Física de la Tierra* **19**,
55-71.

Viana, S., C. Yagüe, and G. Maqueda (2009), Propagation and effects of a mesoscale gravity wave over a weakly-stratified nocturnal boundary layer during the SABLES2006 field campaign, *Bound.-Layer Meteorol.* **133**, 2, 165-188, DOI: 10.1007/s10546-009-9420-4.

Viana, S., E. Terradellas, and C. Yagüe (2010), Analysis of gravity waves generated at the top of a drainage flow, *J. Atmos. Sci.* **67**, 12, 3949-3966, DOI: 10.1175/2010JAS3508.1.

Vickers, D., and L. Mahrt (2003), The cospectral gap and turbulent flux calculations, *J Atmos. Oceanic Technol.* **20**, 5, 660-672, DOI: 10.1175/1520-0426(2003) 20<660:TCGATF>2.0.CO;2.

Voronovich, V., and G. Kiely (2007), On the gap in the spectra of surface-layer atmospheric turbulence, *Bound.-Layer Meteorol.* **122**, 1, 67-83, DOI: 10.1007/s10546-006-9108-y.

Yagüe, C., S. Viana, G. Maqueda, M.F. Lazcano, G. Morales, and J.M. Rees (2007), A study on the nocturnal atmospheric boundary layer: SABLES2006, *Física de la Tierra* **19**, 37-53.

Received 30 January 2011
Received in revised form 8 October 2011
Accepted 17 October 2011